



Published in final edited form as:

Dev Biol. 2018 December 01; 444(Suppl 1): S252–S261. doi:10.1016/j.ydbio.2018.02.016.

Chick cranial neural crest cells use progressive polarity refinement, not contact inhibition of locomotion, to guide their migration

Miriam A. Genuth¹, Christopher D.C. Allen², Takashi Mikawa³, and Orion D. Weiner^{1,*}

¹Cardiovascular Research Institute and Department of Biochemistry and Biophysics, University of California San Francisco, San Francisco, California, United States of America

²Cardiovascular Research Institute and Sandler Asthma Basic Research Center, Department of Anatomy, University of California San Francisco

³Cardiovascular Research Institute, University of California San Francisco

Abstract

To move directionally, cells can bias the generation of protrusions or select among randomly generated protrusions. Here we use 3D two-photon imaging of chick branchial arch 2 directed neural crest cells to probe how these mechanisms contribute to directed movement, whether a subset or the majority of cells polarize during movement, and how the different classes of protrusions relate to one another. We find that, in contrast to *Xenopus*, cells throughout the stream are morphologically polarized along the direction of overall stream movement and do not exhibit contact inhibition of locomotion. Instead chick neural crest cells display a progressive sharpening of the morphological polarity program. Neural crest cells have weak spatial biases in filopodia generation and lifetime. Local bursts of filopodial generation precede the generation of larger protrusions. These larger protrusions are more spatially biased than the filopodia, and the subset of protrusions that are productive for motility are the most polarized of all. Orientation rather than position is the best correlate of the protrusions that are selected for cell guidance. This progressive polarity refinement strategy may enable neural crest cells to efficiently explore their environment and migrate accurately in the face of noisy guidance cues.

Keywords

migration; neural crest; polarity; filopodia; contact inhibition of locomotion

Introduction

Directed cell migration is important for embryonic development, immune function, and wound healing. There are a number of possible strategies that cells can use to generate directed migration. They can read gradients of guidance cues spatially across their surface

*To whom correspondence should be addressed: Orion Weiner, CVRI & Department of Biochemistry and Biophysics, University of California, San Francisco, Cardiovascular Research Building, Room 352F, MC 3120, 555 Mission Bay Blvd. South, San Francisco, CA 94158, Tel. 415-514-4508, Fax 415-514-1176, orion.weiner@ucsf.edu.

(Lauffenburger et al., 1987; Schwarz et al., 2017) and/or compare the concentration of agonist in time (Macnab and Koshland, 1972). Cells can bias the generation of protrusions or select among randomly-generated protrusions. Determining the logical framework cells use for migration is often challenging as it is not readily deduced from knockout phenotypes. However, careful quantitative imaging of migrating cells behavior can be used to discriminate between these migration strategies.

Quantitative imaging has been used to examine the guidance strategies in other migratory cells. Bacteria interpret gradients temporally and accomplish chemotaxis by increasing their run lengths that are directed up the chemoattractant gradient (Berg and Brown, 1972). Eukaryotic cells are capable of interpreting gradients spatially and can spatially bias the generation of protrusions for strong gradients (Arriemerlou and Meyer, 2005; Zigmond, 1974). However, in more shallow gradients, cells show more random protrusion formation and instead spatially bias the selection of protrusions to accomplish directional movement (Andrew and Insall, 2007; Arriemerlou and Meyer, 2005).

Branchial arch (BA) 2 directed neural crest cells migrate from the hindbrain in a dense stream approximately 10 cell layers thick in response to multiple redundant chemoattractants, chemorepellants, extracellular matrix (ECM) cues, and physical barriers. Production of the redundant chemorepellants semaphorin 3A and 3F and the ECM protein versican demarcates the rostral boundary of the BA 2 stream and serves to keep it separate from the BA 1 stream (Eickholt et al., 1999; Gammill et al., 2007; Szabó et al., 2016). The otic placode is thought to provide a physical barrier caudal to the BA2 stream. Sdf-1 is a chemoattractant expressed by the ectoderm that is both overlying and ahead of the neural crest stream (Escot et al., 2013), and a similar role has been proposed for VEGF (McLennan et al., 2010). Inhibition of RhoA in chick or conditional knockout of Rac or Cdc42 in mice fails to disrupt the BA 2 stream organization, suggesting that there could also be significant redundancy in basic cytoskeletal regulation in amniote neural crest (Fuchs et al., 2009; Liu et al., 2013; Rupp and Kulesa, 2007). How chick neural crest cell polarization is regulated remains unknown.

We have some understanding of the molecular logic linking protrusion dynamics to directed migration in *Xenopus* neural crest. These cells make use of a contact inhibition of locomotion (CIL) scheme for their migration (Carmona-Fontaine et al., 2008; Theveneau et al., 2010). CIL is a process in which a cell ceases forward movement upon contact with another cell (Abercrombie and Heaysman, 1953). In the case of sparsely distributed and weakly adhesive cells, CIL often induces the cell to reverse its polarity and move away from the site of contact. However, if the cells are in a very crowded environment, as is the case of *Xenopus* neural crest cells, and/or are strongly adhesive, they may be unable to disengage and will instead maintain contact even after suppression of protrusion formation at the site of contact. In *Xenopus*, cell-cell contact of neural crest cells activates planar cell polarity (PCP) signaling, inducing protrusion retraction at the site of contact (Carmona-Fontaine et al., 2008; Scarpa et al., 2015). As a result of this process, neural crest cells in the middle of the stream are non-polar and non-protrusive while those at the edge of the stream polarize and protrude. These multicellular contacts are necessary for the directed migration of *Xenopus*

neural crest cells. In this setting, guidance cues act by modulating the lifetime of CIL-generated protrusions rather than inducing protrusions *de novo* (Theveneau et al., 2010).

To what extent the *Xenopus* model applies to cranial neural crest cell migration in amniotes is unclear. PCP signaling is required for neural crest migration in *Xenopus* but dispensable for neural crest cell migration in mice (Pryor et al., 2014). While the specific molecular mechanism of *Xenopus* CIL do not appears not to be conserved in mice, it does not exclude the possibility that the *Xenopus* overall strategy for neural crest migration could still apply. Additionally, it has been reported that chick neural crest cells in the middle of the stream commonly have a bipolar morphology (Teddy and Kulesa, 2004), as opposed to the non-polar morphology of *Xenopus* neural crest, suggesting that chick may use a different mechanism than CIL to control overall cell shape during neural crest migration.

To further explore the protrusion dynamics underlying neural crest cell migration we turned to chick as a model capable of live, *in vivo* imaging of migrating neural crest cells (Kulesa and Fraser, 1998). We find that neural crest cells in all regions of the migratory stream have polarized protrusion dynamics relative to the direction of overall stream movement and do not exhibit contact inhibition of locomotion. Neural crest cells show weak spatial biases in filopodia generation and lifetime, stronger biases in the generation of larger protrusions, and are most polarized in their productive protrusions. Thus, chick neural crest cells migrate by conducting a biased search with polarity refinement.

Materials and Methods

Embryos and Electroporations

Fertilized White Leghorn chicken eggs were obtained from Petaluma Farms (Petaluma, CA, USA) and incubated at 38° until Hamburger and Hamilton (HH) stage 8+ to 9 (Hamburger and Hamilton, 1951). A DNA solution consisting of 2.8 ug/uL total DNA (either 2.8 ug/uL of pCAGGS-GAP43-GFP or 2.3 ug/mL pCAGGS-GAP43-GFP and 0.5 ug/uL pCAGGS-H2B-tdTomato) diluted in Pannett-Compton buffer with 1 mg/mL Fast-Green was injected in the lumen of the hindbrain neural tube. Embryos were electroporated *in ovo* using a Nepagene electroporator and BTX model 516 Genetrode 1mm gold plated electrodes positioned 4.5 mm apart parallel to the embryo. Four pulses of 19 V with a 50 millisecond pulse length and a 500 millisecond pulse intervals were used.

Sample preparation for imaging

At HH 11-12, eggs were removed from the incubator and examined. Embryos with sparse but bright labeling of the neural crest were chosen for imaging. Embryos were removed from the egg and placed in EC culture (Chapman et al., 2001). A very thin coat of EC culture was applied to a Bioptechs delta t dish (cat no. 04200417C). Embryos were sandwiched in between two rings of filter paper and clips of tungsten wire were applied to the filter rings to minimize sample drift. In order to prevent motion blur caused by the embryos' heartbeats, the middle of the heart was carefully cut away using tungsten dissection tools 20-60 minutes before the embryo was placed on the microscope.

Two-photon imaging

Embryos were immersed in Pannett-Compton buffer and imaged on an upright LSM 7 MP INDIMO system (Carl Zeiss Microscopy), customized with four GaAsP detectors and a Z-Deck motorized stage (Prior). Samples were imaged with a W Plan-Apochromat 20×/1.0 N.A. water-immersion objective. Excitation was with a Chameleon Ultra II laser (Coherent) tuned to 930 or 940nm, with power attenuated by an acousto-optical modulator. Images were collected with ZEN Black software. A manually adjusted Bioptechs delta t4 culture dish controller was used to maintain the embryos' temperature between 37.5° and 38.5°. 930 nm excitation wavelength was used for samples with GFP alone and 940 nm was used for samples with GFP and tdTomato. 2× frame averaging was performed. For imaging filopodia dynamics, z-stacks with a 1 μm step size were acquired every 30 seconds for 10 minutes. For imaging protrusion dynamics, z-stacks with a 1.5 μm step size were acquired every 3 minutes for at least 2 hours. This slight under-sampling in z allowed for the whole stream to be imaged with minimal neural crest cell death and photobleaching.

Super-resolution Imaging

Embryos were sparsely electroporated with PCAGGS-memGFP and allowed to develop for 10 hours before being fixed in 4% PFA overnight at 4° C. Embryos were washed three times in DPBS for 5 minutes before a segment of the head containing the BA2 stream (roughly from posterior to the otic placode to the midbrain) was excised with a scalpel. This smaller tissue piece was blocked in DPBS with 1% NGS and .1% Triton X-100 for 1 hour at room temperature before being incubated overnight at 4°C with rabbit anti-GFP (1:1000). Tissues were washed and incubated with alexa fluor 488 anti rabbit secondary (1:500), alexa fluor 562 phalloidin (1:500), and hoechst dye (1:5000) at room temperature for two hours. Tissues were mounted dorsal side up in Vectashield antifade mounting media. Small clay spacers were placed under the corners of the coverglass to prevent the tissue from being crushed. Samples were imaged with a Zeiss Airyscan LSM 880 with 405, 488, and 561 lasers, using a 63× objective in fast scan mode. Images were deconvolved using Zen.

Filopodia Polarity Quantification

Filopodia were manually quantified on the z-stack using ImageJ; note that whereas maximum intensity projections are used to represent the stream in some figures, all analysis was done in 3D for quantitation of filopodial polarity. Filopodia were defined as long thin structures less than 1 micron thick. Although filopodia from one cell occasionally contacted the body of another labeled cell, >90% of total filopodia could reliably be assigned based on differences in brightness caused by the heterogeneity of electroporation based gene expression. Nuclei XY position was measured using the Analyze Particles command on a maximum projection. Nuclei Z position was determined manually. Vectors were calculated and the plot was generated using RStudio.

Filopodia Dynamics Quantification

As a quality control, only bright cells with clearly visible filopodia and that were still moving forward at the end of the 10 minutes were quantified. Z-stack timelapses were opened using the FIJI distribution of ImageJ and the Correct 3D Drift plugin was applied to

the raw images. Filopodia were quantified manually on the z-stack using the ROI manager. 8 cells from 3 embryos were analyzed. To aid identification of new filopodia, consecutive frames were overlaid in the green and red channels. To obtain the cell body perimeter, a maximum projection was created of the video and manually thresholded so that the entire cell body was above the threshold. Although filopodia are dimmer than the cell body, many are above the threshold. To remove the remaining filopodia and smooth the cell perimeter, the thresholded image was opened in Matlab and a morphological erosion and opening was performed. The locations of the perimeter pixels were obtained using the boundaries command. The front and back of the cell were defined as respectively, the fourth and first quartile of the perimeter along the direction of overall stream movement (Fig. 3B). This ensured that those quadrants always have an equal length irrespective of cell shape. Rostral and caudal quadrants then occupied the middle of the cell. Quadrant boundaries were recalculated every frame. Filopodia were binned according to which quadrant the base of the filopodium fell into when it was first extended.

For the comparison of the location of filopodia relative to newly generated protrusions, images were processed as above to remove the filopodia. The processed image was used to define an ROI where the new protrusion was extended. These ROIs included on average 11.6% of the cell perimeter. The time the protrusion was first extended was also determined using this processed image. New filopodia were identified without reference to the ROI and then later categorized by whether the nearest perimeter pixel to the base of the filopodium was inside or outside the ROI. 9 protrusions from 8 cells in 5 embryos were analyzed.

3D reconstruction was done using the surfaces tool in Imaris version 8.4.1 (Bitplane).

Statistics were calculated using RStudio.

Protrusion Quantification

Two-photon images were opened in FIJI and the Correct 3D Drift plugin was applied to the images. Cells were chosen for analysis in the first frame of the video based on brightness, separation from other labeled cells, and to ensure sampling of cells from all positions in the migratory stream. Cells that subsequently died or divided were excluded from the analysis. Occasionally during a video, a cell was cut off by stage drift or migrated into a large knot of brightly labeled cells making it difficult to discern its outline. In those cases, only frames where all protrusions could be clearly distinguished were included in the analysis. In total 21 cells from 3 embryos were analyzed.

Protrusions were quantified manually in the z-stack by creating a linear ROI along the length of the protrusion. To exclude retraction tails, protrusions were defined as any structure larger than a filopodium that was actively extended from the cell. Protrusion lifetime was measured from the first frame the protrusion was visible until it started retracting. Productive protrusions were defined as protrusions where the nuclei overlapped the ROI marking the initial protrusion location at some point in the video.

For the quantification of the number of protrusions per cell, a random frame was chosen from three videos at least 15 minutes after their start to avoid ambiguity arising from the presence of a preexisting structure, and then all labeled cells were assayed.

Statistics were calculated using RStudio.

Cell Collision Quantification

A collision event was identified when the leading edge of a protrusion made contact with another labeled cell in at least two z-frames. A protrusion was defined as continuing to extend if at any time point after the collision the leading edge of the protrusion extended farther than it did at the time of contact. The direction of nuclear movement was calculated from two frames prior to the collision to two frames after. False coloring in Fig 2 and 3D reconstruction was done by manually outlining each cell.

Results

Because of the dense packing of neural crest cells during their migration in chick, it is difficult to assay cell morphology when all cells are labeled. To analyze the distribution and dynamics of protrusions in this setting, we labeled a subset of cells in the stream by sparsely electroporating Hamburger and Hamilton (HH) stage 8+ to 9 embryos with pCAGGS-Gap43GFP (mem-GFP to visualize the plasma membrane) and pCAGGS-H2B-tdTomato (to visualize the nuclei) and performed live 3D imaging at HH 11-12 via two-photon microscopy (Fig. 1A). We found that neural crest cells in the BA 2 directed stream displayed a polarized filopodia distribution with more filopodia from the front of the cells than the back relative to the direction of stream movement (Fig. 1A). We calculated an average vector from the nucleus to the filopodia (Fig. 1B) for 128 cells in the embryo shown in Fig. 1A and 60 cells from two additional embryos. Filopodia were defined as any thin protrusions at least 1 micron long and less than 1 micron wide extending out from the cell body. The mean number of filopodia per neural crest cell is 11.1 ± 5.9 . The average filopodia vectors are strongly biased toward the direction of the migration of the overall neural crest stream (Fig. 1D), indicating that neural crest cells are morphologically polarized. Importantly, cells in the middle of the migratory stream have similar filopodial polarity as the cells at the edges of the stream (Fig. 1C, Movie S1). This whole-population polarity is in contrast with the *Xenopus* model (in which interior cells in the stream lack protrusion and polarity).

Given the density of nuclear staining of neural crest cells in the stream, we considered it unlikely that the polarized cells in the middle of the stream consistently lacked contacts at their leading edge. However, to test this possibility we sparsely electroporated embryos with mem-GFP and stained them with phalloidin to label the actin-rich cortex of all neural crest cells. We then imaged the embryos by super-resolution microscopy. We find that even with 40 nm XY and 160 nm Z resolution, it is difficult to distinguish the boundary of one cell from another suggesting that the neural crest stream is an extremely crowded environment with extensive cell contacts (Movie S2). Furthermore, both filopodia and larger protrusions from GFP positive cells made contact with the actin-rich protrusions in other cells (Fig. 2A, Movie S2). These data suggest that unlike *Xenopus*, chick neural crest cells can maintain protrusions even in the presence of extensive cell-cell contact.

To directly assay whether chick neural crest exhibit the behavioral features of contact inhibition of locomotion, we electroporated neural crest cells with mem-GFP and H2B-tdTomato and captured images every 3 minutes to observe the outcome of a protrusion from one labeled cell contacting another labeled cell. Protrusions were defined as any structure larger than a filopodium that was actively extended from the cell body. Only cases where the leading edge of a protrusion made extensive contact with another labeled cell in at least two z-slices were included in our analyses, as we reasoned that these were the situations most likely to induce CIL (Fig. 2B, Movie S3). In two thirds of cases protrusions continued extending post contact (Fig. 2C). The ability of cells to maintain their forward movement following contact coincided with displacement of the cell body (Fig. 2B, frame 1-3) or relied on the three-dimensional context of our assay in which the protrusion moved to slip around the obstructing cell either laterally or in the z-plane (Fig. 2B, frame 3-5). This result is in contrast to most CIL models where contact efficiently induces the collapse of protrusions, as is seen robustly for *Xenopus* neural crest cells (Carmona-Fontaine et al., 2008; Scarpa et al., 2015). We also analyzed the direction of nuclear movement in the protruding cell pre and post collision (Fig. 2C). Regardless of whether we analyzed total protrusions or productive protrusion (Fig. S1), neural crest cells rarely reversed direction post collision with only 17% turning more than 90° ($p < .001$ by Chi squared test). Thus, chick neural crest cells do not exhibit CIL and are likely to employ another strategy to regulate their polarity.

We therefore sought to determine the origin of the polarized distribution of filopodia observed throughout the migratory stream. The biases observed in one point in time could arise from polarized generation of filopodia, polarized maintenance of filopodia, or both. To distinguish between these possibilities, we electroporated neural crest cells with mem-GFP and imaged actively migrating cells every 30 seconds for 10 minutes with a two-photon microscope to capture filopodia dynamics (Fig. 3A and B, Movies S4 and S5).

Filopodia were identified in the z-stack and binned according to the quadrant of the cell in which they were initiated (Fig. 3C). We find that neural crest cells have moderate biases in both filopodia generation and lifetime (Fig. 3D and E). The front quadrant (corresponding to the direction of overall stream migration) has 37% of filopodia generation events, while the back quadrant has 14% of filopodia generation events (Fig. 3D). The rostral and caudal quadrants evenly split the remaining filopodia, with 22% and 27% respectively. Filopodia lifetime exhibits a similar bias with the front quadrant having the longest lived filopodia (mean lifetime of 2.4 minutes), the back the shortest (1.5 minutes), and rostral and caudal having similar, intermediate values (2 and 1.8 minutes respectively) (Fig. 3E). Thus, the robust polarity in filopodia distribution seen at an individual time point (as in Fig. 1D) is a result of both biased filopodia generation as well as biased maintenance.

Filopodia are canonically considered to be sensory structures that cannot generate motility on their own (Jacquemet et al., 2015). We therefore sought to identify a connection between filopodia generation and the creation of larger-scale protrusions. We focused on neural crest cells that were generating new protrusions and quantified the generation of filopodia in the frames preceding protrusion extension. We observed a burst of local filopodia generation preceding protrusion generation by several minutes (Fig. 4A and Movie S6). In the 2.5 minutes before a new protrusion was extended, new filopodia were generated in the local

region where a protrusion will form at more than double the rate per unit of perimeter than in the rest of the cell (Fig. 4B). This suggests a possible connection between the filopodia generation and protrusion generation.

Because filopodia exhibit a spatial bias toward the direction of overall stream migration and filopodia locally correlate with larger protrusion formation, we next sought to analyze the spatial bias in protrusion formation. To quantify large-scale protrusion dynamics, we sparsely electroporated neural crest with mem-GFP and H2B-tdTomato and imaged at least 90% of the neural crest stream in HH 11-12 embryos every three minutes for over two hours (Movies S7 and S8). Protrusions were defined as any structure larger than a filopodium that was actively extended from the cell body. Figure 5A shows a neural crest cell exhibiting typical behaviors such as polarizing, moving forward, and selecting among protrusions. We measured the orientation and active lifetime of 253 protrusions in 21 cells from three embryos. We defined protrusion orientation as the angle from the base of the protrusion to its tip relative to the direction of stream motion. Protrusion orientation was measured at the first frame in which the protrusion was extended. Active protrusion lifetime is the lifetime of the protrusion from birth to the first frame of retraction. Protrusion orientations were heavily biased toward the direction of stream movement (Fig. 5B). They are even more polarized than filopodia generation (Fig. 6C). Cells in the front half of the migratory stream exhibited a similar bias in protrusion orientations to those in the back half of the migratory stream (Fig. S2). Protrusions oriented towards the direction of migration had a longer lifetime than those oriented anti-parallel to the direction of migration (Fig. 5C).

We observed that neural crest cells frequently extend and then retract protrusions without accompanying movement of the cell body (Fig. 5A). We used this behavior to classify protrusions into those that were productive versus non-productive for movement. A productive protrusion was defined as one in which the nucleus of the cell entered the previous position of the protrusion i.e. what was once a protrusion is now the cell body. Productive protrusions make up only 1/3 of the total protrusions. They have orientations that are even more tightly clustered around the direction of stream movement than total protrusions or non-productive protrusions (Fig. 5D and E, Fig. 6C). These observations are consistent with a biased search model where cells efficiently explore their environment by extending multiple protrusions roughly in the desired direction before pruning the losing protrusions.

We were also interested in how such mechanisms could contribute to the cohesiveness of the neural crest stream. Neural crest cells could avoid migrating into inhibitory spaces either by suppressing the generation of protrusions in those directions or by rendering those protrusions non-productive. To address this question, we analyzed the protrusion dynamics of the most rostral and caudal labeled cells of the BA 2 stream. We find that caudally localized neural crest cells have reduced generation of protrusions with a caudal orientation (Fig. S2). This is consistent with the otic placode acting as a physical barrier. In contrast, rostrally localized neural crest cells have no rostral-caudal bias in protrusion generation (Fig. S2). Chemorepellent signaling thus likely acts to bias the selection of productive protrusions rather than biasing protrusion generation.

There are several possible strategies for biasing the selection of protrusions during directional migration. Cells could preferentially select protrusions whose individual orientation matches the desired migration direction or whose absolute position is closest to the ultimate destination (Andrew and Insall, 2007). To address this question for chick neural crest, we quantified the position relative to the center of the nucleus for every protrusion (Fig. 5 and S3). Since protrusion position and orientation were reasonably correlated (Fig. S3), we employed a logistic regression to determine which variable was more predicative of whether a protrusion would be productive. In the linear model, only protrusion orientation had a significant coefficient, suggesting that protrusion orientation is the preferred metric for evaluating protrusion quality (Fig. S3).

We observed that neural crest cells frequently have multiple protrusions (Fig. 5A). This was quantified by counting the number of protrusions on all labeled neural crest cells, in a randomly chosen video frame for three embryos (Fig. 6A). Because the cell must ultimately choose one dominant protrusion to migrate efficiently, we sought to determine whether there is competition among protrusions. Specifically, does the presence of an active, productive protrusion suppress the generation of additional protrusions? To address this question, we measured the average number of additional protrusions generated per 3-minute frame while the cell has no protrusions, a non-productive protrusion, or a productive protrusion. For this analysis, the time the cell was defined as having a protrusion only included frames where the protrusion was not retracting, as we reasoned that a protrusion in the process of being dismantled had already lost the competition. We find no significant difference in the rate of new protrusion generation in a cell with no protrusions or a non-productive protrusion (Fig. 6B). However, the cells with a productive protrusion exhibit decreased generation of other protrusions (Fig. 6B). These data suggest that neural crest cells have a mechanism to evaluate the quality of their existing protrusions when deciding whether to extend new ones.

Discussion

Neural crest cells exhibit progressive sharpening of the polarization of their protrusions in the direction of overall stream migration (Fig. 6C). They have a moderate polarization in filopodia generation that is further sharpened by spatially biased filopodia lifetime to produce a consistently polarized final distribution of filopodia (Fig. 1 and 3) aligned with the overall direction of stream migration. Bursts of local filopodia generation precede the extension of larger protrusions (Fig 4). Total protrusion generation is more polarized than filopodia generation, while productive protrusion orientations are the most highly polarized with 78% of productive protrusions aligned to the direction of stream migration (Fig. 5E and 5C). These data suggest that chick cranial neural crest cell migration through biased search followed by polarity refinement (Fig. 6D). The noisy distribution of filopodia generation allows neural crest cells to explore many possible directions for migration. The bias in filopodia lifetime further refines the region of search. The locations of high filopodial density generate larger protrusions, and a subset of the protrusions that are best aligned with the external guidance cues are used to direct migration. Productive protrusions suppress the generation of new protrusions to enable processive movement (Leithner et al., 2016). This is a continuous process with cells constantly extending and retracting all different types of protrusions as they migrate. This progressive polarity refinement strategy may enable neural

crest cells to efficiently explore their environment and migrate accurately in the face of noisy guidance cues.

Xenopus and chick neural crest cells represent two different approaches for mesenchymal cell stream migration. In Xenopus, neural crest cells migrate as a zippered together stream in which only cells at the edge of the migratory stream are protrusive (Theveneau et al., 2010). These edge cells are then the ones that interpret guidance cues, since they principally act to modulate the lifetime of pre-existing, CIL generated protrusions (Theveneau et al., 2010). Zebrafish neural crest cells are similar to Xenopus in their requirement for PCP dependent CIL for migration, suggesting that the Xenopus model also applies to them (Matthews et al., 2008; Moore et al., 2013; Theveneau et al., 2010). In contrast, chick neural crest cells do not exhibit the CIL—they continue to protrude and migrate in the same direction following contact with one another (Fig 2, Fig S1, Movies S2 and S3) in contrast to the repulsive behavior that characterizes CIL. For chick, neural crest cells in all positions of the migratory stream are polarized and protrusive, suggesting that they all could be interpreting guidance signals. The spatial biases observed in both protrusion generation and lifetime indicate that both steps could be subject to regulation. Interestingly, mice do not need PCP signaling for neural crest migration, suggesting that their neural crest may behave more like chick (Pryor et al., 2014). Whether mouse neural crest cells have a pattern of cell polarity more similar to that of chick or Xenopus remains to be determined. Chick thus provides a model for characterizing an alternate strategy for neural crest cell migration that is still amenable to powerful live-imaging techniques.

The molecular mechanisms underlying the protrusion dynamics of neural crest cells remain to be determined. The actin cytoskeleton is an excitable system that can in some cells generate protrusions spontaneously (Devreotes et al., 2017). Is this the source of neural crest cells' multiplicity of protrusions? If so, how do productive protrusions suppress the generation of new protrusions? This could be accomplished by robust chemoattractant signaling in productive protrusions either generating a long range negative inhibitor of actin polymerization (Houk et al., 2012) or by sequestering a limited pool of positive regulator. *In vivo* imaging of cytoskeletal and signaling reporters and manipulation of potential guidance cues will likely provide new insights into the molecular mechanisms of amniote neural crest cell migration.

A major open question is whether chick neural crest cells individually interpret external chemotactic cues or whether cells share information to migrate collectively. Migrating chick neural crest cells express a variety of cell communication molecules including cadherins, ephrins and Eph receptors, raising the possibility that homotypic interactions could alter neural crest cell behavior (Chalpe et al., 2010; Mellott and Burke, 2008; Nakagawa and Takeichi, 1998). However, the density of the neural crest stream combined with the complicated shapes of individual neural crest cells make it challenging to rigorously distinguish sites of interaction from non-interaction (Movie S2). Although the lack of repulsion and protrusion suppression indicate that chick neural crest cells do not exhibit CIL (Fig. 2), it is possible that these protrusions are still involved in other forms of cell-cell communication and alignment of cell polarity in the stream. Perturbative experiments of candidate communication molecules or labeling schemes that enable visualization of

individual cell boundaries in dense stream (Loulier et al., 2014) will be necessary to reveal whether neural crest cells share information through cell-cell contact.

A further issue is whether neural crest cells in all regions of the migratory stream use the same migration mechanisms. Neural crest cells at the front of the stream have a different gene expression signature from those in the back (McLennan et al., 2015a, 2015b, 2012). Mathematical models have been developed that suggest that neural cell migration makes use of two populations of cells, leaders that directly interpret the gradient, and followers that follow the leaders (McLennan et al., 2015a; Wynn et al., 2013). Additionally, it has been reported that neural crest cells in different regions of the migratory stream have different morphologies with cells at the front being non-polar 'hairy cells' while cells at the back have a bipolar morphology (Teddy and Kulesa, 2004). In contrast, we observe no difference in neural crest cell protrusive behavior between cells in the front and those at the back (Fig 1C and S2). This discrepancy may be due to a difference in the embryonic stage chosen for analysis as Teddy and Kulesa conducted their analysis up to 7 hours later than our experiments at HH 11-12. Alternatively, as large scale mixing has been observed between cells within the stream, there may be no distinct leader and follower cell populations (Richardson et al., 2016), or perhaps the gene expression differences at different portions of the stream don't result in differences in migratory behavior. While our data is consistent with an absence of specialized leader cells, future studies should combine individual cell and regional-specific perturbations with our quantitative analyses of cell dynamics to further investigate this question.

Supplementary Material

Refer to Web version on PubMed Central for supplementary material.

Acknowledgments

We thank Xin-Zi Tang and Sara Venters for helpful discussion, Rieko Asai for technical help, Rieko Asai and Lisandro Maya-Ramos for a critical reading of the manuscript, and the Cardiovascular Research Institute for financial support of the two-photon.

Funding: This work was supported by the National Institutes of Health (NIH) [R35GM118167] and an American Heart Association Established Investigator Award to ODW; and NIH [R37HL078921, R01HL122375, and R01HL132832] to TM.

References

- Abercrombie M, Heaysman JEM. 1953; Observations on the social behaviour of cells in tissue culture: I. Speed of movement of chick heart fibroblasts in relation to their mutual contacts. *Exp Cell Res.* 5:111–131. DOI: 10.1016/0014-4827(53)90098-6 [PubMed: 13083622]
- Andrew N, Insall RH. 2007; Chemotaxis in shallow gradients is mediated independently of PtdIns 3-kinase by biased choices between random protrusions. *Nat Cell Biol.* 9:193–200. DOI: 10.1038/ncb1536 [PubMed: 17220879]
- Arrieumerlou C, Meyer T. 2005; A Local Coupling Model and Compass Parameter for Eukaryotic Chemotaxis. *Dev Cell.* 8:215–227. DOI: 10.1016/j.devcel.2004.12.007 [PubMed: 15691763]
- Berg HC, Brown DA. 1972; Chemotaxis in *Escherichia coli* analysed by three-dimensional tracking. *Nature.* 239:500–504. [PubMed: 4563019]

- Carmona-Fontaine C, Matthews HK, Kuriyama S, Moreno M, Dunn GA, Parsons M, Stern CD, Mayor R. 2008; Contact inhibition of locomotion in vivo controls neural crest directional migration. *Nature*. 456:957–961. DOI: 10.1038/nature07441 [PubMed: 19078960]
- Chalpe AJ, Prasad M, Henke AJ, Paulson AF. 2010; Regulation of cadherin expression in the chicken neural crest by the Wnt/B-catenin signaling pathway. *Cell Adhes Migr*. 4:431–438. DOI: 10.4161/cam.4.3.12138
- Chapman SC, Collignon J, Schoenwolf GC, Lumsden A. 2001; Improved method for chick whole-embryo culture using a filter paper carrier. *Dev Dyn*. 220:284–289. DOI: 10.1002/1097-0177(20010301)220:3<284::AID-DVDY1102>3.0.CO;2-5 [PubMed: 11241836]
- Devreotes PN, Bhattacharya S, Edwards M, Iglesias PA, Lampert T, Miao Y. 2017; Excitable Signal Transduction Networks in Directed Cell Migration. *Annu Rev Cell Dev Biol*. 33:103–125. DOI: 10.1146/annurev-cellbio-100616-060739 [PubMed: 28793794]
- Eickholt BJ, Mackenzie SL, Graham A, Walsh FS, Doherty P. 1999; Evidence for collapsin-1 functioning in the control of neural crest migration in both trunk and hindbrain regions. *Development*. 126:2181–2189. [PubMed: 10207143]
- Escot S, Blavet C, Härtle S, Duband JL, Fournier-Thibault C. 2013; Misregulation of SDF1-CXCR4 Signaling Impairs Early Cardiac Neural Crest Cell Migration Leading to Conotruncal Defects. *Circ Res*. 113:505–516. DOI: 10.1161/CIRCRESAHA.113.301333 [PubMed: 23838132]
- Fuchs S, Herzog D, Sumara G, Büchmann-Møller S, Civenni G, Wu X, Chrostek-Grashoff A, Suter U, Ricci R, Relvas JB, Brakebusch C, Sommer L. 2009; Stage-Specific Control of Neural Crest Stem Cell Proliferation by the Small Rho GTPases Cdc42 and Rac1. *Cell Stem Cell*. 4:236–247. DOI: 10.1016/j.stem.2009.01.017 [PubMed: 19265663]
- Gammill LS, Gonzalez C, Bronner-Fraser M. 2007; Neuropilin 2/semaphorin 3F signaling is essential for cranial neural crest migration and trigeminal ganglion condensation. *Dev Neurobiol*. 67:47–56. DOI: 10.1002/dneu.20326 [PubMed: 17443771]
- Hamburger V, Hamilton HL. 1951; A series of normal stages in the development of the chick embryo. *J Morphol*. 88:49–92. DOI: 10.1002/jmor.1050880104 [PubMed: 24539719]
- Houk AR, Jilkine A, Mejean CO, Boltyanskiy R, Dufresne ER, Angenent SB, Altschuler SJ, Wu LF, Weiner OD. 2012; Membrane tension maintains cell polarity by confining signals to the leading edge during neutrophil migration. *Cell*. 148:175–188. DOI: 10.1016/j.cell.2011.10.050 [PubMed: 22265410]
- Jacquemet G, Hamidi H, Ivaska J. 2015; Filopodia in cell adhesion, 3D migration and cancer cell invasion. *Curr Opin Cell Biol, Cell adhesion and migration*. 36:23–31. DOI: 10.1016/j.ceb.2015.06.007
- Kulesa PM, Fraser SE. 1998; Neural Crest Cell Dynamics Revealed by Time-Lapse Video Microscopy of Whole Embryo Chick Explant Cultures. *Dev Biol*. 204:327–344. DOI: 10.1006/dbio.1998.9082 [PubMed: 9882474]
- Lauffenburger D, Farrell B, Tranquillo R, Kistler A, Zigmond S. 1987; Gradient perception by neutrophil leucocytes, continued. *J Cell Sci*. 88:415–416. [PubMed: 3503899]
- Leithner A, Eichner A, Müller J, Reversat A, Brown M, Schwarz J, Merrin J, de Gorter DJJ, Schur F, Bayerl J, de Vries I, Wieser S, Hauschild R, Lai FPL, Moser M, Kerjaschki D, Rottner K, Small JV, Stradal TEB, Sixt M. 2016; Diversified actin protrusions promote environmental exploration but are dispensable for locomotion of leukocytes. *Nat Cell Biol*. 18:1253–1259. DOI: 10.1038/ncb3426 [PubMed: 27775702]
- Liu Y, Jin Y, Li J, Seto E, Kuo E, Yu W, Schwartz RJ, Blazo M, Zhang SL, Peng X. 2013; Inactivation of Cdc42 in neural crest cells causes craniofacial and cardiovascular morphogenesis defects. *Dev Biol*. 383:239–252. DOI: 10.1016/j.ydbio.2013.09.013 [PubMed: 24056078]
- Loulier K, Barry R, Mahou P, Le Franc Y, Supatto W, Matho KS, Ieng S, Fouquet S, Dupin E, Benosman R, Chédotal A, Beaurepaire E, Morin X, Livet J. 2014; Multiplex Cell and Lineage Tracking with Combinatorial Labels. *Neuron*. 81:505–520. DOI: 10.1016/j.neuron.2013.12.016 [PubMed: 24507188]
- Macnab RM, Koshland DE. 1972; The Gradient-Sensing Mechanism in Bacterial Chemotaxis. *Proc Natl Acad Sci U S A*. 69:2509–2512. [PubMed: 4560688]

- Matthews HK, Marchant L, Carmona-Fontaine C, Kuriyama S, Larraín J, Holt MR, Parsons M, Mayor R. 2008; Directional migration of neural crest cells in vivo is regulated by Syndecan-4/Rac1 and non-canonical Wnt signaling/RhoA. *Development*. 135:1771–1780. DOI: 10.1242/dev.017350 [PubMed: 18403410]
- McLennan R, Dyson L, Prather KW, Morrison JA, Baker RE, Maini PK, Kulesa PM. 2012; Multiscale mechanisms of cell migration during development: theory and experiment. *Development*. 139:2935–2944. DOI: 10.1242/dev.081471 [PubMed: 22764050]
- McLennan R, Schumacher LJ, Morrison JA, Teddy JM, Ridenour DA, Box AC, Semerad CL, Li H, McDowell W, Kay D, Maini PK, Baker RE, Kulesa PM. 2015a; Neural crest migration is driven by a few trailblazer cells with a unique molecular signature narrowly confined to the invasive front. *Development*. 142:2014–2025. DOI: 10.1242/dev.117507 [PubMed: 25977364]
- McLennan R, Schumacher LJ, Morrison JA, Teddy JM, Ridenour DA, Box AC, Semerad CL, Li H, McDowell W, Kay D, Maini PK, Baker RE, Kulesa PM. 2015b; VEGF signals induce trailblazer cell identity that drives neural crest migration. *Dev Biol*. 407:12–25. DOI: 10.1016/j.ydbio.2015.08.011 [PubMed: 26278036]
- McLennan R, Teddy JM, Kasemeier-Kulesa JC, Romine MH, Kulesa PM. 2010; Vascular endothelial growth factor (VEGF) regulates cranial neural crest migration in vivo. *Dev Biol*. 339:114–125. DOI: 10.1016/j.ydbio.2009.12.022 [PubMed: 20036652]
- Mellott DO, Burke RD. 2008; Divergent roles for Eph and ephrin in avian cranial neural crest. *BMC Dev Biol*. 8:56.doi: 10.1186/1471-213X-8-56 [PubMed: 18495033]
- Moore R, Theveneau E, Pozzi S, Alexandre P, Richardson J, Merks A, Parsons M, Kashef J, Linker C, Mayor R. 2013; Par3 controls neural crest migration by promoting microtubule catastrophe during contact inhibition of locomotion. *Development*. 140:4763–4775. DOI: 10.1242/dev.098509 [PubMed: 24173803]
- Nakagawa S, Takeichi M. 1998; Neural crest emigration from the neural tube depends on regulated cadherin expression. *Development*. 125:2963–2971. [PubMed: 9655818]
- Pryor SE, Massa V, Savery D, Andre P, Yang Y, Greene NDE, Copp AJ. 2014; Vangl-dependent planar cell polarity signalling is not required for neural crest migration in mammals. *Development*. 141:3153–3158. DOI: 10.1242/dev.111427 [PubMed: 25038043]
- Richardson, J; Gauert, A; Briones Montecinos, L; Fanlo, L; Alhashem, ZM; Assar, R; Marti, E; Kabla, A; Härtel, S; Linker, C. Leader Cells Define Directionality of Trunk, but Not Cranial, Neural Crest Cell Migration. *Cell Rep*. 2016.
- Rupp PA, Kulesa PM. 2007; A role for RhoA in the two-phase migratory pattern of post-otic neural crest cells. *Dev Biol*. 311:159–171. DOI: 10.1016/j.ydbio.2007.08.027 [PubMed: 17900555]
- Scarpa E, Szabó A, Bibonne A, Theveneau E, Parsons M, Mayor R. 2015; Cadherin Switch during EMT in Neural Crest Cells Leads to Contact Inhibition of Locomotion via Repolarization of Forces. *Dev Cell*. 34:421–434. DOI: 10.1016/j.devcel.2015.06.012 [PubMed: 26235046]
- Schwarz J, Bierbaum V, Vaahtomeri K, Hauschild R, Brown M, de Vries I, Leithner A, Reversat A, Merrin J, Tarrant T, Bollenbach T, Sixt M. 2017; Dendritic Cells Interpret Haptotactic Chemokine Gradients in a Manner Governed by Signal-to-Noise Ratio and Dependent on GRK6. *Curr Biol*. 27:1314–1325. DOI: 10.1016/j.cub.2017.04.004 [PubMed: 28457871]
- Szabó A, Melchionda M, Nastasi G, Woods ML, Campo S, Perris R, Mayor R. 2016; In vivo confinement promotes collective migration of neural crest cells. *J Cell Biol*. 213:543–555. DOI: 10.1083/jcb.201602083 [PubMed: 27241911]
- Teddy JM, Kulesa PM. 2004; In vivo evidence for short- and long-range cell communication in cranial neural crest cells. *Development*. 131:6141–6151. DOI: 10.1242/dev.01534 [PubMed: 15548586]
- Theveneau E, Marchant L, Kuriyama S, Gull M, Moepps B, Parsons M, Mayor R. 2010; Collective chemotaxis requires contact-dependent cell polarity. *Dev Cell*. 19:39–53. DOI: 10.1016/j.devcel.2010.06.012 [PubMed: 20643349]
- Wynn ML, Rupp P, Trainor PA, Schnell S, Kulesa PM. 2013; Follow-the-leader cell migration requires biased cell-cell contact and local microenvironmental signals. *Phys Biol*. 10:35003.doi: 10.1088/1478-3975/10/3/035003
- Zigmond SH. 1974; Mechanisms of sensing chemical gradients by polymorphonuclear leukocytes. *Nature*. 249:450–452. [PubMed: 4834231]

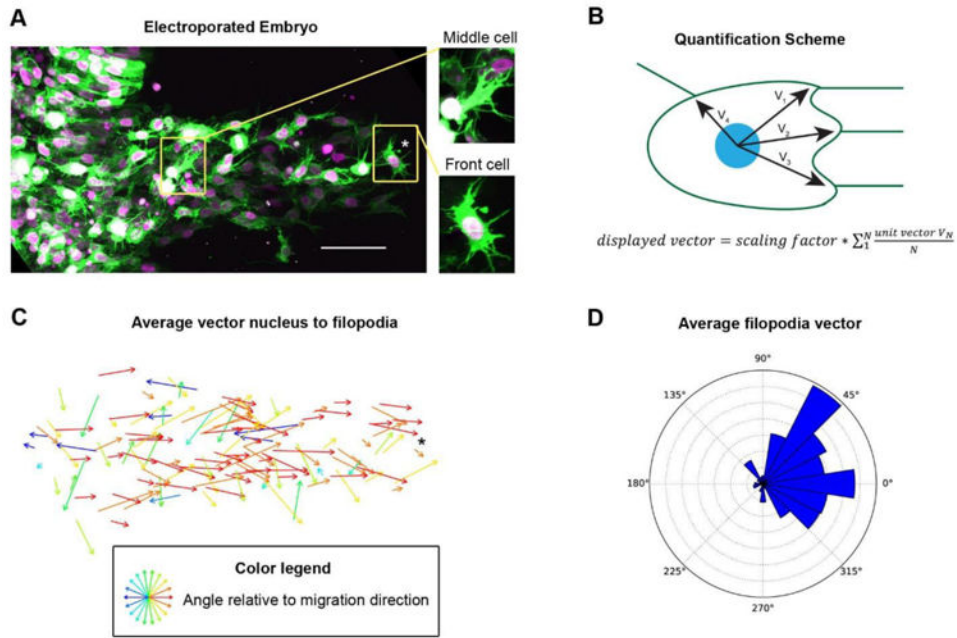


Figure 1. Neural crest cells throughout the migration stream are polarized

(A) HH 12 Embryo electroporated with pCAGGS-GAP43-GFP (mem-GFP, to label plasma membrane) and pCAGGS-H2B-tdTomato (to label the nucleus) was imaged live by two-photon microscopy; Image is a maximum intensity projection of 92 1 μm z-planes scale bar, 50 μm , insets are cell in middle and front of the stream. Corresponds to Movie S1.

(B) Quantification scheme of average filopodia position vector. The angular position of the base of each filopodia to the nucleus relative to the direction of overall stream migration was measured in 2D (though filopodial assignment to each cell was made in 3D). The vectors were all assigned a length of 1 and an average vector was calculated. Scaling factor is for visibility in plot.

(C) Plot of vectors calculated as in panel B for 128 neural crest cells from embryo shown in panel A. Asterisk marks a cell near the front of the stream (in both 1A and 1C as a fiducial mark). Neural crest cells throughout the stream have more filopodia on their surface facing the direction of overall stream migration compared to other directions ($p < .001$ by Rao's spacing test). See also Movie S1.

(D) Weighted rose plot of average filopodia position for 188 neural crest cells from three embryos. Plot is weighted so all embryos contribute equally.

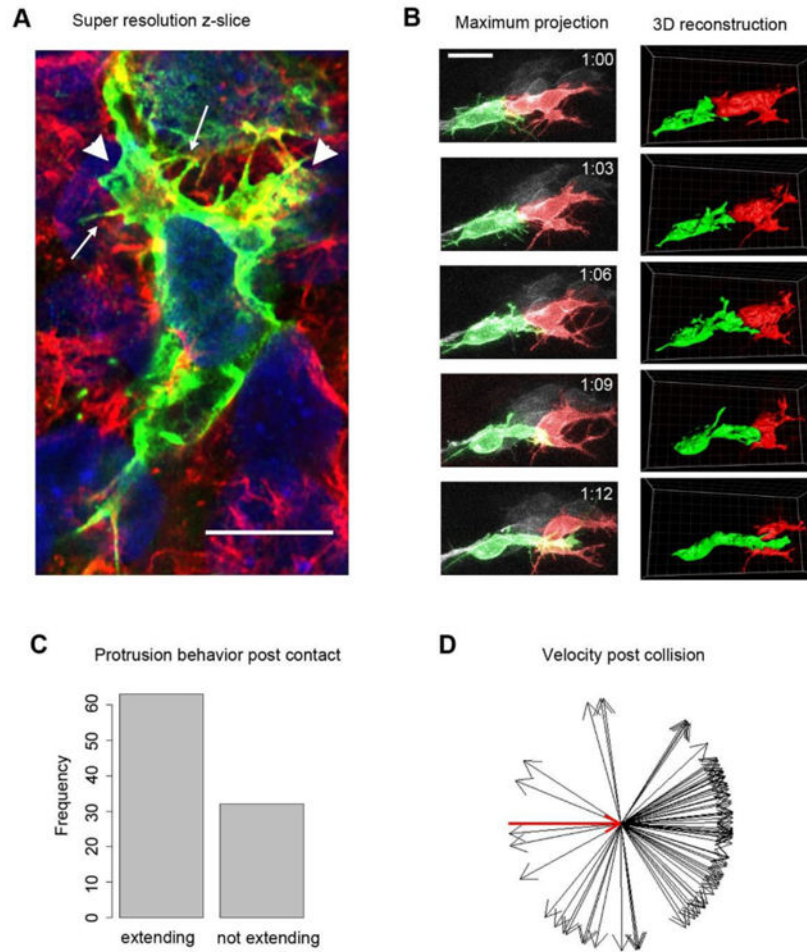


Figure 2. Neural crest do not exhibit contact inhibition of locomotion

(A) Single 160 nm z-slice super-resolution imaging of a whole mount embryo electroporated with mem-GFP and stained with 488 anti GFP (to sparsely label cells and more clearly visualize individual protrusions) and 562 phalloidin to label filamentous actin, and hoescht to label the nuclei. Note that all protrusions on GFP positive cell are making contact with other cells. Arrows mark filopodia, and arrowheads mark two larger protrusions. Scale bar, 10 μ m. Corresponds to Movie S2.

(B) Pseudocolored two photon timelapse of a collision between two mem-GFP labeled cells. The trailing cell, in green, protrudes into and then over the lead cell. Time in hours. Scale bar, 20 μ m. Corresponds to Movie S3.

(C) Fate of protrusions following contact with another labeled cell. Two thirds of protrusions continue to extend. N=95 collision events involving 81 protrusions in 19 cells in 3 embryos.

(D) Directional vectors of nuclear movement post-contact relative to pre-contact. Red arrow marks the normalized pre-contact vector. Neural crest cells rarely reverse direction even following head-on contact between a protrusion and another labeled cell. A similar trend is seen when the analysis is restricted to productive protrusions (Fig. S1). N=86 collision events.

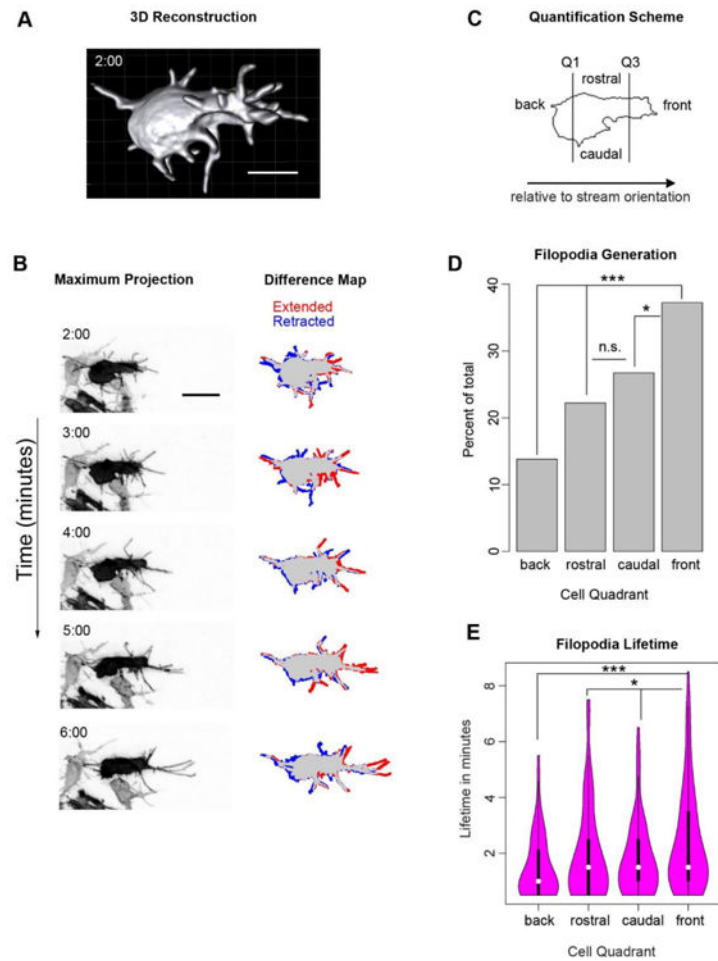


Figure 3. Both the generation and lifetime of neural crest filopodia are biased towards the direction of overall stream migration

(A) Still image from Movie S4 of a 3D reconstruction of a neural crest cell showing the extensive filopodial extensions and complex 3D morphology of neural crest cells in vivo. Scale bar, 10 μm .

(B) Still images from Movie S5 of a neural crest cell electroporated with pCAGGS-mem-GFP and imaged every 30 seconds for 10 minutes to investigate filopodial dynamics. This is the same cell as that shown in panel A. The difference map shows a comparison of the current frame with the image taken one minute previously, with regions that were extended and retracted labeled with red and blue respectively. Time in minutes; scale bar, 20 μm .

(C) Quantification scheme for filopodia spatial distribution used in graphs D and E. The perimeter of the cell body, excluding filopodia, was determined in every frame and divided into quadrants. The front and back quadrants each have $\frac{1}{4}$ of the total perimeter while rostral and caudal split the remaining half.

(D) (D and E) Filopodial generation events (D) and the lifetime of these filopodia (E) based on the quadrant where the filopodium was initiated. The direction of overall stream migration (front) has a significantly higher rate of filopodial generation and longer-lived filopodia relative to the back and sides. N=333 filopodia from 8 cells in 3 embryos. * $p < .05$, *** $p < .001$ by Chi-square (D) or Mann-Whitney U (E).

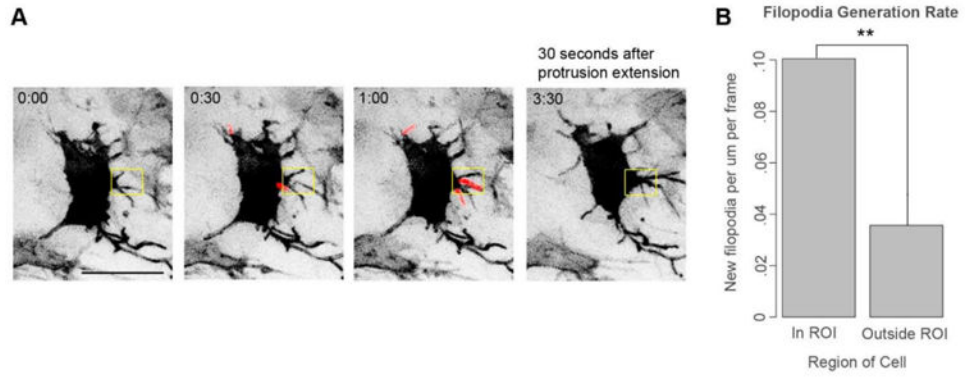


Figure 4. Neural crest cells locally generate a burst of filopodia before extending larger protrusions

(A) Still images from Movie S6 of a neural crest cell electroporated with pCAGGS-mem-GFP and imaged every 30 seconds. New filopodia are highlighted in red. Box is an ROI bracketing where the new protrusion will emerge. Scale bar, 20 μm .

(B) Quantification of local filopodia generation rate prior to the generation of the new protrusion. Newly-generated filopodia were identified in the z-stack for 2.5 minutes prior to the extension of the protrusion. The filopodia generation rate in the ROI and the rest of the cell was calculated as a function of the cell perimeter length in those compartments. We quantified 9 protrusion generation events in 8 cells in 5 embryos. Filopodia were generated in the region where a new protrusion will emerge at more than double the expected rate compared to other areas of the cell. ** $p < .01$ by paired t-test.

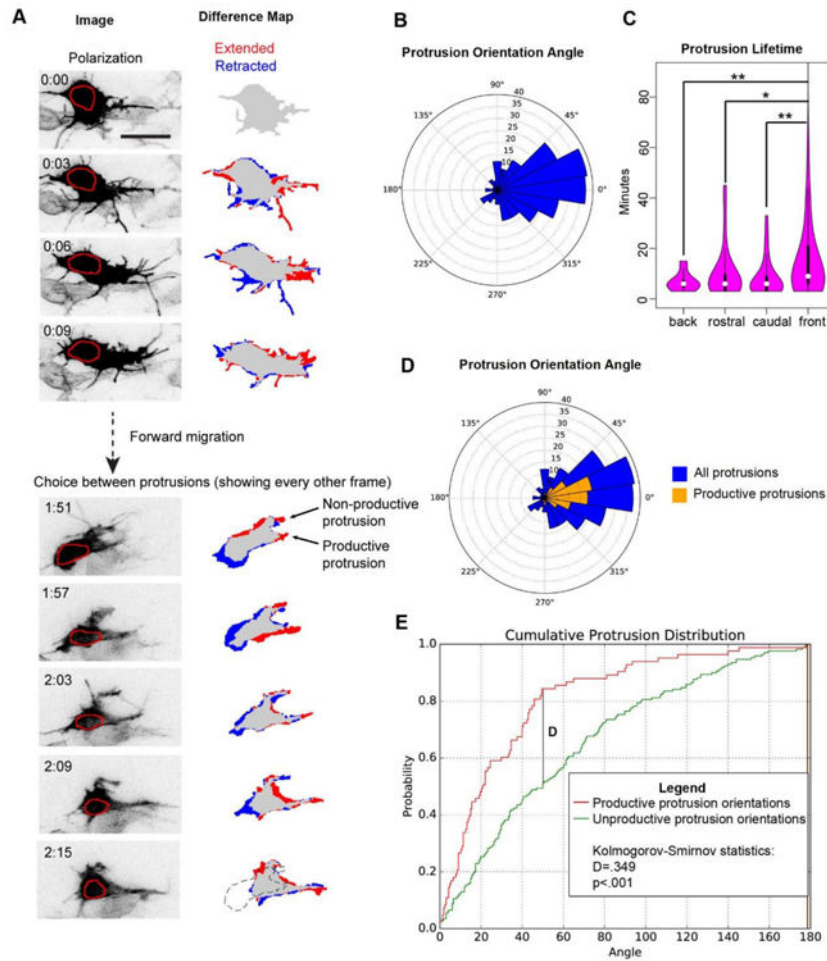


Figure 5. Neural crest cells migrate by biasing both protrusion generation and retraction

(A) Representative images of a neural crest cell from Movie S7 electroporated with pCAGGS-mem-GFP and pCAGGS-H2B-tdTomato and imaged every 3 minutes. The red circle outlines the nucleus. This cell exhibits typical neural crest cell behaviors such as polarization, forward migration, and choice among multiple protrusions. Difference map shows a comparison of the current frame with either the image taken three minutes earlier for the analysis of polarization (top panels) or six minutes earlier in the analysis of choice between protrusions (bottom panels), with regions that were extended and retracted labeled red and blue respectively. Dotted outline is silhouette of cell at 1:51. Time in hours:mins, scale bar 20 μ m. See Movie S7 and S8.

(B) Quantification of protrusion orientation angle in HH11-12 embryos. N=253 protrusions from 21 cells in 3 embryos. Protrusion angles are strongly polarized towards the direction of overall stream migration ($p < .001$ by Kolmogorov-Smirnov compared to a uniform distribution).

(C) Protrusion lifetime, excluding frames when the protrusion is being retracted. Protrusions were binned by angle relative to the direction of stream movement. * $p < .05$, ** $p < .01$ by Mann-Whitney U. Protrusions aligned toward the direction of overall stream movement have longer lifetimes than those protrusions that point in other directions.

(D) Orientation angle of all protrusions (blue) and productive protrusions (gold). Productive protrusions were defined as ones where the nucleus enters the region that the protrusion was; i.e. what was once a protrusion is now the cell body.

(E) Normalized cumulative histogram of productive and non-productive protrusion orientations. Protrusion orientations were collapsed to 0° to 180° to enable the use of more standard statistical tests. Productive protrusion orientations were more tightly clustered around the direction of overall stream movement than non-productive protrusions.

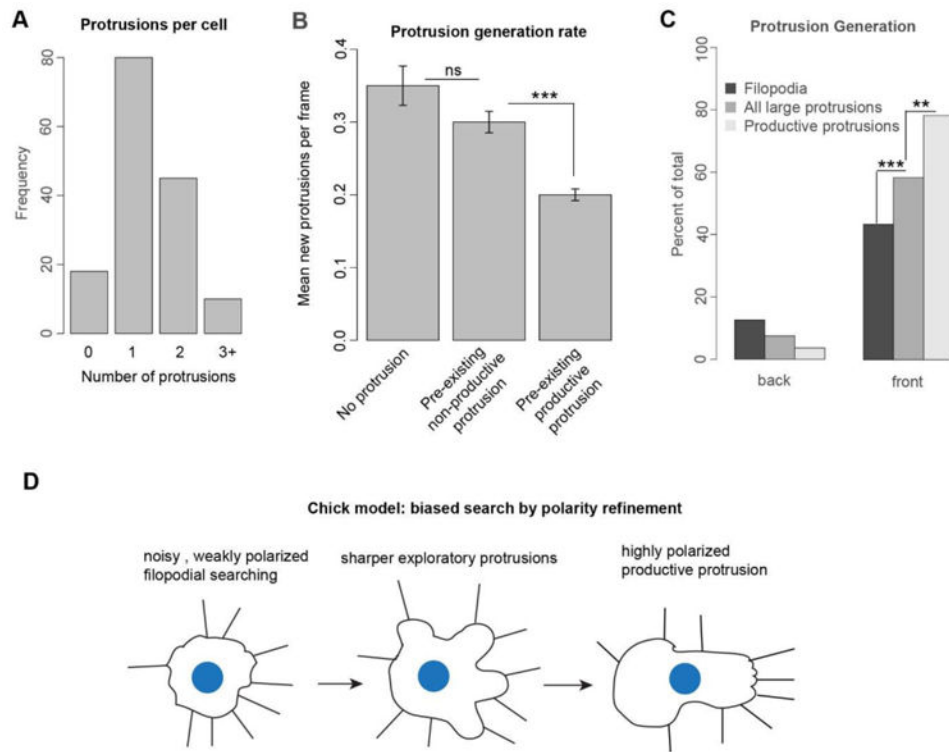


Figure 6. Neural crest cells exhibit competition among protrusions

(A) Number of protrusions per neural crest cell. All labeled neural crest cells, 153 in total, were quantified in a randomly chosen frame for 3 embryos.

(B) Average number of protrusions generated in a 3 minute frame given the protrusive state of the cell. Neural crest cells either have no protrusions, a pre-existing not retracting *productive* protrusion, or a preexisting not retracting *non-productive* protrusion. Cells with productive protrusions have a lower rate of generating new protrusions. Error bars are Poisson s.e.m. ns is not significant. *** $p < .001$ by Poisson rate-ratio test.

(C) Comparison of the generation rate for filopodia, all protrusions, and productive protrusions towards or away from the direction of overall stream migration. Structures are binned as in Fig. 4B and 5C. There is a successive sharpening of polarization for filopodia generation, all protrusion generation, and productive protrusion generation. ** $p < .01$, *** $p < .001$, by Fisher Exact test

(D) Model for chick neural crest cell migration. Chick neural crest cells migrate by progressively refining the polarity of their protrusions.